Journal of Sound and Vibration (2001) **248**(3), 533–556
doi:10.1006/jsvi.2001.3803, available online at http://www.idealibrary.com on IDEAL®

ANALYTICAL SOLUTION ON THE DRAGGED SURGE VIBRATION OF TENSION LEG PLATFORMS (TLPS) WITH WAVE LARGE BODY AND SMALL BODY MULTI-INTERACTIONS

H. H. Lee and W.-S. Wang

Department of Marine Environment and Engineering, National Sun Yat-sen University, Kaohsiung, Taiwan, Republic of China. E-mail: hhlee@mail.nsysu.edu.tw

(*Received* 15 *May* 2001, *and in final form* 22 *May* 2001)

This paper presents a complete analytical solution for the dynamic behavior of both the platform and tethers in the tension-leg platform system when the platform system is subjected to the wave-induced surge motion and the flow-induced drag motion. Along with the analysis the coupling problem of a two-dimensional tension leg platform interacting with a monochromatic linear wave train in an inviscid and incompressible fluid is considered. Both the scattering problem and the radiation problem are combined together with the equation of motion for the platform and the one for the tether to solve for all unknowns in the flow field and for the response of the platform system. The dynamic behavior of the platform and tethers is realized from these solutions. The material property of the tether and the dimensional effect for the platform and the tether are both taken into account in the analytical analysis. The convergence of the solution is verified and the results are further compared with the case without considering the drag effect. It is found that the non-linear drag effect is significant when the draft or the dimension of the platform structure is small and furthermore, the variation of material properties and dimension of tether also affect the dynamic behavior of both the tether and the platform itself.

1. INTRODUCTION

Tension leg platforms (TLPs) are usually used as a working station for oil exploration in deep water. Lately, the application of this structural system has been extended into newly developed facilities such as the floating breakwater system and the fish-farming cage system. The TLPs consist of a semi-submerged structure and pretensioned tethers anchored to the ocean bed. The difficulty in the dynamic analysis of the TLPs is due to the non-linearity of the TLP motion and the boundary conditions on the free surface and on the structural bottom [1]. For this problem the linear boundary value problem is incorporated into a scattering problem and a radiation problem [2]. This problem was solved by a numerical method in the 1970s [3, 4], and also studied in an experimental test [4]. Recently, an analytical solution was proposed and demonstrated by Lee and Lee [5], in which the surge motion of platform with pretensioned tethers was calculated. In that study, however, the elasticity of tethers was only implied and the motion of tethers was simplified as on-line rigid-body motion proportional to the top platform to estimate the pretension force while the drag effect was ignored. Thus, both the material property and the mechanical behavior for the tether incorporated in the tension-leg platform system were ignored. When this simplification was applied, no matter what material was used or what the dimension of

0022-460X/01/480533 + 24 $35.00/0

tethers was, the dynamic response of the platform would remain the same in terms of the vibration mode, periods and the vibration amplitude. This is not true for the actual engineering application.

The drag effect on the TLP system is the other important issue. Even though many researches carried out have put efforts on the tether drag effect, the interactions between wave and platform (large body) were generally ignored in those researches. Without considering the interaction between the structure and the wave, some numerical studies were presented lately, such as the study on coupled six degrees of rigid-body motion for the platform [6] and the simulation for the platform system by using a three-dimensional element [7]. It is rarely that for the study of TLP system the interactions among the wave, platform structure and the tethers are all included. Some trials have been made, for instance, Lee [8] presented a method to include the drag effect. In that study, a linear profile along the water depth was assumed for the tension leg tethers and then without solving the tether motion the drag force was integrated along the tether. Lee *et al.* [9] tried to find the drag motion of the tethers when the interactions between wave and platform were considered. In that study, however, only surge motion was considered for the platform and the drag tether motion was obtained separately after the motion of the platform was realized.

Therefore, in this study it is attempted to solve the whole TLP system in a complete analytical scheme in which the problem involves the aforementioned wave, large body and small body multi-interactions and furthermore the material properties of the tether are accounted for. The equation of the motion and the corresponding solution for both the platform and the tethers of the tension leg platform system subjected to flow-induced drag motion were derived and solved. Based on previous studied [5, 9] the equations for the scattering problem and the radiation problem were established on the boundaries in terms of the velocity potentials. These equations were combined into the equation of motion for the tether and the equation for the platform motion and then solved simultaneously to obtain the flow field, platform responses and the tether motion. It is the purpose of this study to examine the influence of the tether drag effect on the platform motion when the true behavior of the tethers is included in the solution. Along with the solution that presented as the comparison of the responses between the platform with and without tether drags, the influence of parameters of the platform structure, the water wave and the tension leg tethers is also studied. It is found from the numerical results that the drag effect of tethers reduces the platform motion a great deal and the tether drag is also influenced significantly by the parameters of the platform structure, water waves and the tethers. When the platform locates in deep water or the platform has shallow draft or small dimension, the engineering design and calculation without considering the tether drag effect may significantly overestimate the platform responses.

2. GENERAL WAVE THEORY

For the inviscid and incompressible fluid and irrotational flow, a single-valued velocity potential ϕ can be defined as

$$\mathbf{u} = -\nabla\phi, \tag{1}$$

where u is the flow velocity, ∇ the gradient operator. The velocity potential satisfies the Laplace equation

$$\nabla^2\phi = 0 \tag{2}$$

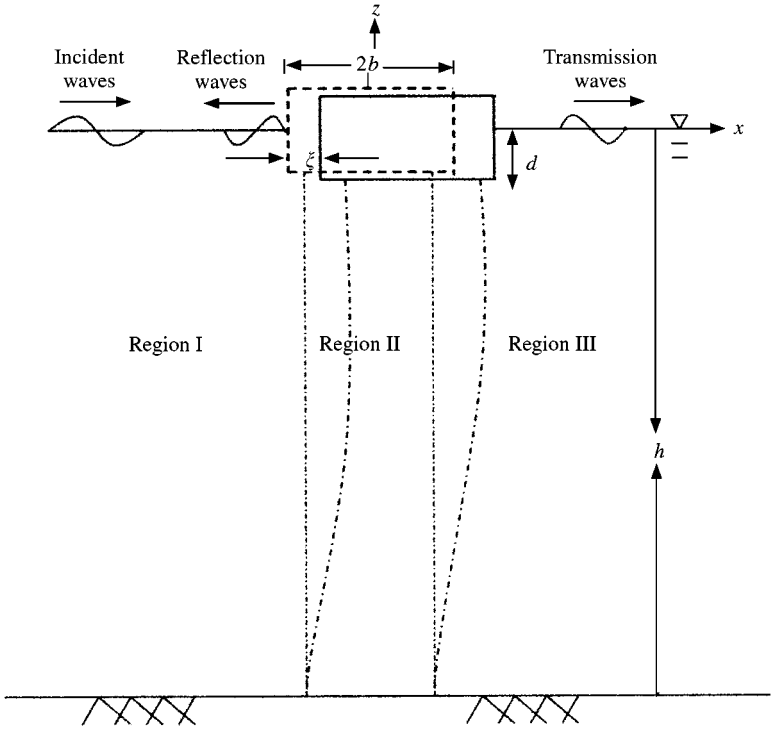

Figure 1. Definition sketch of the TLP problem.

and the Bernoulli equation

$$-\frac{\partial \phi}{\partial t} + \frac{1}{2}\nabla\phi \cdot \nabla\phi + \frac{p}{\rho_w} + gz = 0 \tag{3}$$

in the flow field, where p is the pressure and ρ_w is the water density. The non-linear term in equation (3) is neglected when the linear small amplitude wave is assumed.

A two-dimensional tension leg platform interacting with a monochromatic small amplitude wave propagating in the $+x$ direction was considered here as was shown in Figure 1. The wave form and the associated velocity potential are given accordingly as

$$\eta_i = -\mathrm{i}A_i \mathrm{e}^{-(K_1 x + \mathrm{i}\sigma t)} \tag{4}$$

and

$$\phi_i = \frac{A_i g}{\sigma} \frac{\cos[K_1(z+h)]}{\cos(K_1 h)} \mathrm{e}^{-(K_1 x + \mathrm{i}\sigma t)}, \tag{5}$$

where A_i is the wave amplitude, g is the gravitational constant, h is the water depth, $\sigma = (2\pi/T)$ is the angular frequency with T as the period, and $k_1 = -\mathrm{i}k$, where $k = (2\pi/L)$ is the wave number with L as the wavelength. K_1 satisfies the dispersion relation

$$\sigma^2 = -gK_1 \tan(K_1 h). \tag{6}$$

3. TENSION-LEG PLATFORM SYSTEM

In the platform system, the motion of the structure induced by the small amplitude incident wave is assumed to be small. The wave-induced structural motion can be solved from the imposed boundary problem. Because of the linearity of the problem, the problem can be incorporated into a scattering and a radiation problem [10]. The wave force calculated from the scattering problem provides the force function in the radiation problem, and the forced oscillation then generates outgoing waves.

A tension leg platform system is illustrated in Figure 1, where the flow field is divided into three regions with two artificial boundaries at $x = -b$ and b. In region **I**, the total velocity potential ϕ_{I} consists of incident waves ϕ_i, scattered waves ϕ_{Is}, and radiated waves ϕ_{Iw}. In regions II and III, the total velocity potentials ϕ_{II} and ϕ_{III} consists of scattered waves ϕ_{IIs} and ϕ_{IIIs}, and radiated waves ϕ_{IIw} and ϕ_{IIIw}. The subscript s denotes the scattering problem and w denotes the radiation (wave making) problem. All of the velocity potentials satisfy the Laplace equation. Furthermore, Sommerfeld's radiation condition is satisfied at the infinity of regions I and III to secure unique solutions,

$$\lim_{x \to \pm\infty} \left[\frac{\partial \phi}{\partial x} \pm \frac{1}{c} \frac{\partial \phi}{\partial t} \right] = 0, \tag{7}$$

where c is the celerity of the travelling waves.

3.1. SCATTERING PROBLEM

In the scattering problem, the incident wave is diffracted by a fixed structure. The corresponding boundary value problem is also shown in Figure 1. Applying the method of the separation of variables, matching the horizontal boundary conditions in each region, and applying Sommerfeld's condition to regions I and III, the corresponding surface elevation and velocity potential can be found as follows.

In region I:

$$\phi_{\mathrm{Is}} = \sum_{n=1}^{\infty} \frac{A_{\mathrm{Is}n} g}{\sigma} \frac{\cos[K_n(z+h)]}{\cos(K_n h)} \mathrm{e}^{[K_n(x+b) - \mathrm{i}\sigma t]} \tag{8}$$

and

$$\eta_{\mathrm{Is}} = -\mathrm{i} \sum_{n=1}^{\infty} A_{\mathrm{Is}n} \mathrm{e}^{[Kn(x+b) - \mathrm{i}\sigma t]}. \tag{9}$$

In region III:

$$\phi_{\mathrm{IIIs}} = \sum_{n=1}^{\infty} \frac{A_{\mathrm{IIIs}n} g}{\sigma} \frac{\cos[K_n(z+h)]}{\cos(K_n h)} \mathrm{e}^{-[K_n(x-b) + \mathrm{i}\sigma t]} \tag{10}$$

and

$$\eta_{\mathrm{IIIs}} = -\mathrm{i} \sum_{n=1}^{\infty} A_{\mathrm{IIIs}n} \mathrm{e}^{-[K_n(x-b) + \mathrm{i}\sigma t]}, \tag{11}$$

where the eigenvalues K_n can be solved from the dispersion equation

$$\sigma^2 = gK_n \tan(K_n h) \tag{12}$$

with

$$K_1 = -\mathrm{i}k \quad \text{for } n = 1, \qquad (2n-3)\frac{\pi}{2} < K_n h < (n-1)\pi. \tag{13}$$

In region II:

$$\phi_{\mathrm{IIs}} = \frac{\mathrm{i}g}{\sigma}\left[\left(A_{\mathrm{IIs}P1}\frac{x}{b} + A_{\mathrm{IIs}N1}\right)\cos K_{\mathrm{II}1}(z+h) + \sum_{n=2}^{\infty}(-1)^{n-1}(A_{\mathrm{IIs}Pn}\mathrm{e}^{-K_{\mathrm{II}n}(x+b)} + A_{\mathrm{IIs}Nn}\mathrm{e}^{K_{\mathrm{II}n}(x-b)})\cos K_{\mathrm{II}n}(z+h)\right]\mathrm{e}^{-\mathrm{i}\sigma t}, \tag{14}$$

where the eigenvalues $K_{\mathrm{II}n}$ can be solved from the dispersion equation

$$K_{\mathrm{II}n} = \frac{(n-1)\pi}{h-d}, \quad n \geqslant 1. \tag{15}$$

The series of four unknowns $A_{\mathrm{Is}n}, A_{\mathrm{IIs}Pn}, A_{\mathrm{IIIs}n}, A_{\mathrm{IIs}Nn}$ can further be solved from the $4N$ sets of equations derived from two artificial boundaries of region II, as follows.

The kinematic boundary conditions at $x = -b$:

$$\frac{\partial(\phi_i + \phi_{\mathrm{Is}})}{\partial x} = 0, \quad 0 < z < -d \tag{16}$$

and

$$\frac{\partial(\phi_i + \phi_{\mathrm{Is}})}{\partial x} = \frac{\partial \phi_{\mathrm{IIs}}}{\partial x}, \quad -h < z < -d. \tag{17}$$

The dynamic boundary conditions at $x = -b$:

$$\frac{\partial(\phi_i + \phi_{\mathrm{Is}})}{\partial t} = \frac{\partial \phi_{\mathrm{IIs}}}{\partial t}, \quad -h < z < -d. \tag{18}$$

The kinematic boundary conditions at $x = +b$:

$$\frac{\partial \phi_{\mathrm{IIIs}}}{\partial x} = 0, \quad 0 < z < -d \tag{19}$$

and

$$\frac{\partial \phi_{\mathrm{IIs}}}{\partial x} = \frac{\partial \phi_{\mathrm{IIIs}}}{\partial x}, \quad -h < z < -d. \tag{20}$$

The dynamic boundary conditions at $x = +b$:

$$\frac{\partial \phi_{\mathrm{IIs}}}{\partial t} = \frac{\partial \phi_{\mathrm{IIIs}}}{\partial t}, \quad -h < z < -d. \tag{21}$$

Now by applying the orthogonal properties between the functions, the $4N$ sets of boundary conditions are written when $\alpha = 1$ as follows.

The kinematic boundary conditions at $x = -b$:

$$\frac{K_\alpha \langle Z_\alpha Z_\alpha \rangle}{\cos K_\alpha h} A_{\mathrm{I}s\alpha} - \mathrm{i}\left[\frac{1}{b}\langle Z_{\mathrm{II}1} Z_\alpha \rangle^d A_{\mathrm{II}sP1} + \sum_{n=2}^{\infty} (-1)^{n-1} K_{\mathrm{II}n} \langle Z_{\mathrm{II}n} \rangle \right.$$

$$\left. (-A_{\mathrm{II}sPn} + \mathrm{e}^{-2K_{\mathrm{II}n}b} A_{\mathrm{II}sNn}) \right] = \delta_{\alpha 1} \mathrm{e}^{K1b} \frac{K_1 \langle Z_1 Z_1 \rangle}{\cos(K_1 h)} A_i. \tag{22}$$

The dynamic boundary conditions at $x = -b$:

$$-\mathrm{i} \sum_{n=1}^{\infty} \frac{\langle Z_{\mathrm{II}\alpha} Z_n \rangle}{\cos(K_n h)} A_{\mathrm{I}sn} - \langle Z_{\mathrm{II}\alpha} Z_{\mathrm{II}\alpha} \rangle \{ [(1-\delta_{\alpha 1})(-1)^{\alpha-1} - \delta_{\alpha 1}] A_{\mathrm{II}sP\alpha}$$

$$+ [(1-\delta_{\alpha 1})(-1)^{\alpha-1} + \delta_{\alpha 1}] \mathrm{e}^{-2K_{\mathrm{II}\alpha}b} A_{\mathrm{II}sNa} \} = \mathrm{i}\mathrm{e}^{K_1 b} \frac{\langle Z_{\mathrm{II}\alpha} Z_1 \rangle^d}{\cos(K_1 h)} A_i. \tag{23}$$

The kinematic boundary conditions at $x = +b$:

$$\mathrm{i} \frac{\langle Z_{\mathrm{II}1} Z_\alpha \rangle}{b} A_{\mathrm{II}sP1} + \mathrm{i} \sum_{n=2}^{\infty} [(-1)^{n-1} K_{\mathrm{II}n} \langle Z_{\mathrm{II}n} Z_\alpha \rangle^d (\mathrm{e}^{-2K_{\mathrm{II}n}b} A_{\mathrm{II}sPn}$$

$$+ A_{\mathrm{II}sNn})] + \frac{K_\alpha \langle Z_\alpha z_\alpha \rangle}{\cos(K_\alpha h)} A_{\mathrm{III}sP\alpha} = 0. \tag{24}$$

The dynamic boundary conditions at $x = +b$:

$$\langle Z_{\mathrm{II}\alpha} Z_{\mathrm{II}\alpha} \rangle^d \{ [(1-\delta_{\alpha 1})(-1)^{\alpha-1} + \delta_{\alpha 1}] (\mathrm{e}^{-2K_{\mathrm{II}\alpha}b} A_{\mathrm{II}sP\alpha} + A_{\mathrm{II}sN\alpha}) \}$$

$$+ \mathrm{i} \sum_{n=1}^{\infty} \frac{\langle Z_{\mathrm{II}\alpha} Z_n \rangle^d}{\cos(K_n h)} A_{\mathrm{III}sn} = 0, \tag{25}$$

where δ is the Kronecker delta and $\langle Z_* \rangle$ and $\langle Z_* Z_* \rangle$ are defined in Appendix A.

3.2. RADIATION PROBLEM

The structure is considered to be forced in motion by the wave force induced by incident waves and scattered waves. The corresponding boundary value problem is illustrated in Figure 2. The displacement of the dragged surge motion is given by

$$\xi = S\mathrm{e}^{-\mathrm{i}\sigma t}, \tag{26}$$

where S is the unknown amplitude of the surge motion.

By means of a method similar to the scattering problem and applying the radiation condition on the infinite boundary, the solutions of the radiation problem are written as follows.

In region I:

$$\phi_{\mathrm{I}w} = \sum_{n=1}^{\infty} \frac{A_{\mathrm{I}wn} g}{\sigma} \frac{\cos[K_n(z+h)]}{\cos(K_n h)} \mathrm{e}^{[K_n(x+b) - \mathrm{i}\sigma t]}, \tag{27}$$

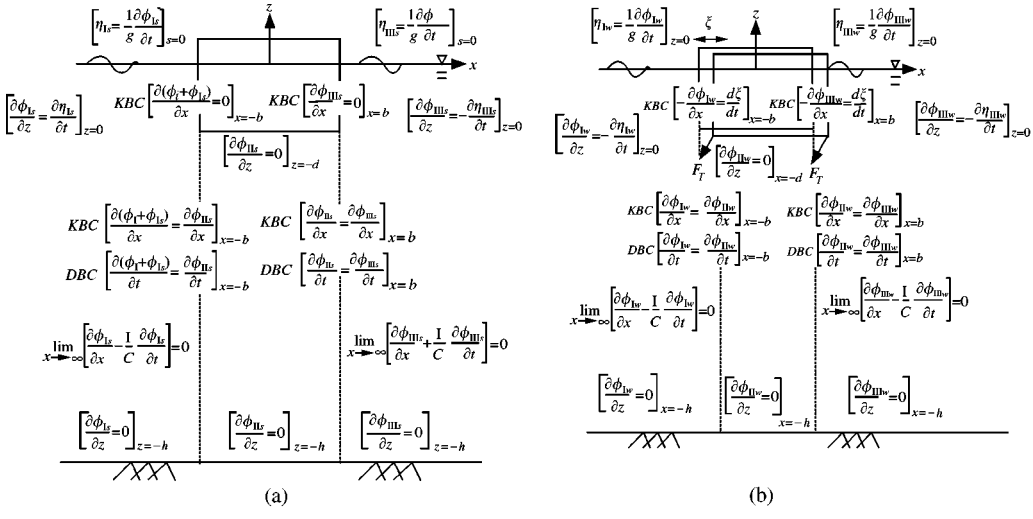

Figure 2. Illustration of boundary conditions for (a) the scattering problem, (b) the radiation problem.

$$\eta_{\mathrm{I}w} = -\mathrm{i}\sum_{j=1}^{\infty} A_{\mathrm{I}wn}\mathrm{e}^{[K_n(x+b)-\mathrm{i}\sigma t]}. \tag{28}$$

In region III:

$$\phi_{\mathrm{III}w} = \sum_{n=1}^{\infty} \frac{A_{\mathrm{III}wn}g}{\sigma}\frac{\cos[K_n(z+h)]}{\cos(K_n h)}\mathrm{e}^{-[K_n(x-b)+\mathrm{i}\sigma t]}, \tag{29}$$

$$\eta_{\mathrm{III}w} = -\mathrm{i}\sum_{n=1}^{\infty} A_{\mathrm{III}wn}\mathrm{e}^{-[K_n(x-b)+\mathrm{i}\sigma t]}. \tag{30}$$

In region II:

$$\phi_{\mathrm{II}w} = \frac{\mathrm{i}g}{\sigma}\left[\left(A_{\mathrm{II}wP1}\frac{x}{b} + A_{\mathrm{II}wN1}\right)\cos K_{\mathrm{II}1}(z+h) + \sum_{n=2}^{\infty}(-1)^{n-1}(A_{\mathrm{II}wPn}\mathrm{e}^{-K_{\mathrm{II}n}(x+b)} + A_{\mathrm{II}wNn}\mathrm{e}^{K_{\mathrm{II}n}(x-b)})\cos K_{\mathrm{II}n}(z+h)\right]\mathrm{e}^{-\mathrm{i}\sigma t}. \tag{31}$$

Again four series of unknown amplitudes of waves $A_{\mathrm{I}wn}, A_{\mathrm{II}wPn}, A_{\mathrm{II}wNn}, A_{\mathrm{III}wn}$ can be solved from the four sets of equations derived from two vertical boundaries. After applying the orthogonalities for the related functions the boundary conditions were rearranged and presented as follows.

The kinematic boundary conditions at $x = -b$:

$$\frac{K_\alpha\langle Z_\alpha Z_\alpha\rangle}{\cos K_\alpha h}A_{\mathrm{I}w\alpha} - \mathrm{i}\left[\frac{1}{b}\langle Z_{\mathrm{II}1}Z_\alpha\rangle^d A_{\mathrm{II}wP1} + \sum_{n=2}^{\infty}(-1)^{n-1}K_{\mathrm{II}n}\langle Z_{\mathrm{II}n}Z_\alpha\rangle^d (-A_{\mathrm{II}wPn} + \mathrm{e}^{-2K_{\mathrm{II}n}b}A_{\mathrm{II}wNn})\right] - \frac{\mathrm{i}\sigma^2}{g}\langle Z_\alpha^0\rangle S = 0. \tag{32}$$

The dynamic boundary conditions at $x = -b$:

$$-\mathrm{i}\sum_{n=1}^{\infty}\frac{\langle Z_{\mathrm{II}\alpha}Z_n\rangle^d}{\cos(K_n h)}A_{\mathrm{I}wn} - \langle Z_{\mathrm{II}\alpha}Z_{\mathrm{II}\alpha}\rangle^d\{[(1-\delta_{\alpha 1})(-1)^{\alpha-1}-\delta_{\alpha 1}]A_{\mathrm{II}wP\alpha} + [(1-\delta_{\alpha 1})(-1)^{\alpha-1}+\delta_{\alpha 1}]\mathrm{e}^{-2K_{\mathrm{II}\alpha}b}A_{\mathrm{II}wN\alpha}\} = 0. \tag{33}$$

The kinematic boundary conditions at $x = +b$:

$$\mathrm{i}\frac{\langle Z_{\mathrm{II}1}Z_\alpha\rangle^d}{b}A_{\mathrm{II}wP1} + \mathrm{i}\sum_{n=2}^{\infty}[(-1)^{n-1}K_{\mathrm{II}n}\langle Z_{\mathrm{II}n}Z_\alpha\rangle^d(-\mathrm{e}^{-2K_{\mathrm{II}n}b}A_{\mathrm{II}wPn} + A_{\mathrm{II}wNn})] + \frac{K_\alpha\langle Z_\alpha Z_\alpha\rangle}{\cos(K_\alpha h)}A_{\mathrm{III}wP\alpha} + \frac{\mathrm{i}\sigma^2}{g}\langle Z_\alpha^0\rangle S = 0. \tag{34}$$

The dynamic boundary conditions at $x = +b$:

$$\langle Z_{\mathrm{II}\alpha}Z_{\mathrm{II}\alpha}\rangle^d\{[(1-\delta_{\alpha 1})(-1)^{\alpha-1}+\delta_{\alpha 1}](\mathrm{e}^{-2K_{\mathrm{II}\alpha}b}A_{\mathrm{II}wP\alpha} + A_{\mathrm{II}wN\alpha})\} + \mathrm{i}\sum_{n=1}^{\infty}\frac{\langle Z_{\mathrm{II}\alpha}Z_n\rangle^d}{\cos(K_n h)}A_{\mathrm{III}wn} = 0, \tag{35}$$

where $\langle Z_* Z_*\rangle$ are also defined in Appendix A. To solve for the unknown amplitude S of the surge motion as shown in kinematic boundary conditions, the equation of surge motion of the structure was required.

3.3. GENERAL MOTION OF THE PLATFORM

The equation of motion of the platform structure derived from Newton's second law is written to include both the wave force on the large body and the drag on the tension leg tethers, when the dynamic tension of order ξ^2 is neglected, as

$$M\frac{\mathrm{d}^2\xi}{\mathrm{d}t^2} + K^*\xi = F_w + F_{d1} + F_{d2}, \tag{36}$$

where M is the mass of the platform structure and K^* is the equivalent stiffness of the platform system induced by the pre-tensioned tethers. F_w is the horizontal wave force acting on two vertical sides of the structure, while F_{d1} and F_{d2} are wave forces exerted on the first and second tether of the tension leg respectively.

The equivalent stiffness of the platform system is presented [11], when the material property and the tether dimension are taken into account, as

$$K^* = \frac{2\rho_w g b}{\ell}(d - d_0)\left(\frac{\mu}{\mu+1}\right), \tag{37}$$

where $\ell = h - d$, $d_0 = M/(2\rho_w b)$, d_0 and d are the drafts of the structure before and after applying the pre-tension force. μ is the proportional stiffness parameter defined as the ratio between the tether stiffness and the buoyancy force of the platform structure submerged in the water of unit depth such as

$$\mu = \frac{EA_t/\ell}{2\rho_w g b}, \tag{38}$$

where E is Young's modulus of the tether dependent on the material property and A_t is the cross-sectional area of the tether. It is noted that when the rigid-body property was assumed for the tether, a very large value of E such that $\mu \to \infty$ and that the equivalent stiffness of the platform system reduced into a traditional form as $K^* = (2\rho_w g b/\ell)(d - d_0)$.

The wave force F_w can be obtained through the integration of the total hydrodynamic pressure over the vertical surfaces of the structure at $x = -b$ and b (from the linearized Bernoulli equation), as

$$F_w = \rho_w \int_{-d}^{0} \left(\frac{\partial \phi_{\mathrm{I}}}{\partial t}\bigg|_{x=-b} - \frac{\partial \phi_{\mathrm{III}}}{\partial t}\bigg|_{x=b} \right) \mathrm{d}z. \tag{39}$$

The theorem of waves on the small body is adopted for forces F_{d1} and F_{d2} on the tether, which can be obtained through the modified Morison's equation [12, 13] accounting for relative motions between fluid and tether as

$$F_{d1/d2} = \int_{-h}^{-d} [0{\cdot}5\rho_w D C_d |u - \dot{\chi}|(u - \dot{\chi}) + 0{\cdot}25\pi\rho_w D^2 C_m(\dot{u} - \ddot{\chi}) + 0{\cdot}25\pi\rho_w D^2 \ddot{\chi}]\,\mathrm{d}z, \tag{40}$$

where D is the diameter of the tension leg; C_d the drag coefficient; C_m the inertia coefficient and u and $\dot{u}$ are the velocity and acceleration of the fluid, respectively, while $\dot{\chi}$ and $\ddot{\chi}$ are velocity and acceleration of the tension leg tethers. It is noticed that the coefficients C_d and C_m are taken as constants when considering only the local acceleration term [14] and therefore the integration can be carried out. It is also noted that in the first term of the right-hand side, the non-linear drag was shown and the linear drag coefficient Rd^* was presented by adopting Lorent's hypothesis of equivalent work within one period of waves [15] as

$$Rd^* = \frac{\int_{-h}^{-d}\int_0^T \{[0{\cdot}5\rho_w D C_d |u - \dot{\chi}|(u - \dot{\chi})](u - \dot{\chi})\}\,\mathrm{d}t\,\mathrm{d}z}{\int_{-h}^{-d}\int_0^T [\rho_w D\sigma(u - \dot{\chi})(u - \dot{\chi})]\,\mathrm{d}t\,\mathrm{d}z}. \tag{41}$$

By substituting back into the modified Morison's equation, the wave forces on the tether are rewritten as

$$F_{d1\,d2} = \int_{-h}^{-d} [\rho_w D\sigma Rd^*(u - \dot{\chi}) + 0{\cdot}25\pi\rho_w D^2 C_m(\dot{u} - \ddot{\chi}) + 0{\cdot}25\pi\rho_w D^2 \ddot{\chi}]\,\mathrm{d}z. \tag{42}$$

To apply these drag forces to the equation of motion for the platform, the motion of the tethers of the tension leg must be obtained simultaneously. Thus, the equation of motion for the pretension tethers was presented subsequently as follows.

3.4. MOTION OF THE PRETENSION TETHERS

The equation of motion for each pretension tether subjected to the wave-induced forces and surge motion of top platform can be written as

$$\rho \frac{\partial^2 \chi}{\partial t^2} + C \frac{\partial \chi}{\partial t} - T^* \frac{\partial^2 \chi}{\partial z^2} = f_d, \tag{43}$$

where χ is the horizontal deflection of the tether, ρ is the mass of unit length of tether, T^* is the pretension force in the platform system and C is the damping coefficient of unit length of tether. Similarly, the unit length wave force exerted on the tether is obtained through Morison's equation for small body while the relative motion between the fluid and the tether is accounted for. As was presented in equation (40) and then modified in equation (42) without the integration along the water depth, the unit length wave force f_d is shown as

$$f_d = \rho_w D\sigma Rd^{**}(u - \dot{\chi}) + 0{\cdot}25\pi\rho_w D^2 C_m(\dot{u} - \ddot{\chi}) + 0{\cdot}25\pi\rho_w D^2\ddot{\chi}, \tag{44}$$

where

$$Rd^{**} = \frac{\int_0^T \{[0{\cdot}5\rho_w DC_d|u - \dot{\chi}|(u - \dot{\chi})](u - \dot{\chi})\}\,\mathrm{d}t}{\int_0^T [\rho_w D\sigma(u - \dot{\chi})(u - \dot{\chi})]\,\mathrm{d}t}$$

After substitution of equation (44), equation (43) can be rewritten in the form

$$[\rho + 0{\cdot}25\pi\rho_w D^2(C_m - 1)]\frac{\partial^2\chi}{\partial t^2} + (C + Rd^{**}\rho_w D\sigma)\frac{\partial\chi}{\partial t}$$

$$- T^*\frac{\partial^2\chi}{\partial z^2} = 0{\cdot}25\pi\rho_w D^2 C_m\dot{u} + Rd^{**}\rho_w D\sigma u. \tag{45}$$

The velocity of fluid in the equation is obtained from the potential, as was obtained in the large-body problem combined with the scattering and the radiation problem, thus $u = -\partial\phi_{\mathrm{II}}/\partial x$ and $\dot{u} = \partial u/\partial t$. Substituting u and $\dot{u}$ into equation (45) we have

$$[\rho + 0{\cdot}25\pi\rho_w D^2(C_m - 1)]\frac{\partial^2\chi}{\partial t^2} + (C + Rd^{**}\rho_w D\sigma)\frac{\partial\chi}{\partial t} - T^*\frac{\partial^2\chi}{\partial z^2}$$

$$= -(0{\cdot}25\pi\rho_w D^2 C_m g + \mathrm{i}Rd^{**}g\rho_w D)\left\{\frac{A_{\mathrm{IIs/}wP1}}{b}\cos K_{\mathrm{II}1}(z + h)\right.$$

$$\left. + \sum_{n=2}^{\infty}(-1)^{n-1}(-K_{\mathrm{II}n}A_{\mathrm{IIs/}wPn} + K_{\mathrm{IIs/}wNn}\mathrm{e}^{-2bK_{\mathrm{II}n}})\cos K_{\mathrm{II}n}(z + h)\right\}\mathrm{e}^{-\mathrm{i}\sigma t}. \tag{46}$$

The motion of the tether at the joint connected to the platform structure will be the same as the motion of the platform that was assumed to be harmonic with amplitude S and frequency σ, as $\chi(-d, t) = \mathrm{Se}^{-\mathrm{i}\sigma t}$, and at the sea bed the motion is restrained thus, $\chi(-h, t) = 0$. Assuming that the motion of the tether is in the same harmonic form as the platform $\chi(z, t) = Z(z)\mathrm{e}^{-\mathrm{i}\sigma t}$, and substituting back in the equation of motion, a reduced equation of motion for the tether is given by

$$T^*\frac{\mathrm{d}^2 Z}{\mathrm{d}z^2} + \{[\rho + 0{\cdot}25\pi\rho_w D^2(C_m - 1)]\sigma^2 + (C + Rd^{**}\rho_w D\sigma)(\mathrm{i}\sigma)^2\}Z(z)$$

$$= (0{\cdot}25\pi\rho_w D^2 C_m g + \mathrm{i}Rd^{**}g\rho_w D)\left\{\frac{A_{\mathrm{IIs/}wP1}}{b}\cos K_{\mathrm{II}1}(z + h)\right.$$

$$\left. + \sum_{n=2}^{\infty}(-1)^{n-1}(-K_{\mathrm{II}n}A_{\mathrm{IIs/}wPn} + K_{\mathrm{IIs/}wNn}\mathrm{e}^{-2bK_{\mathrm{II}n}})\cos K_{\mathrm{II}n}(z + h)\right\} \tag{47}$$

with reduced boundary conditions

$$Z(-d) = S, \quad Z(-h) = 0. \tag{48}$$

Now equation (47) is an ordinary differential equation and ready to be solved into the following form:

$$Z(z) = C_1 e^{az} + C_2 e^{-az} + \sum_{n=1}^{\infty} a_n \cos K_{IIn}(n+h), \tag{49}$$

where C_1, C_2, a, and a_n are given in Appendix B. Accordingly, the deflection function for the tension leg tether related to the flow field region II is established as

$$\chi(z,t) = \left[C_1 e^{az} + C_2 e^{-az} + \sum_{n=1}^{\infty} a_n \cos K_{IIn}(z+h) \right] e^{-i\sigma t}. \tag{50}$$

A similar relationship can be established for the tether of right-hand side with coefficients in the equation as C_1^*, C_2^*, a^*, and a_n^*, which are also shown in Appendix B. Now with the motion of the tether and the velocity potential for the wave a complete equation of motion for the platform structure can be established with interactions among the platform, wave and tension leg tethers.

3.5. COMPLETE EQUATION OF MOTION OF PLATFORM

The equation of motion for the platform as presented in equation (36) can be further modified while the displacement for the pretension tethers is obtained by using equation (50) and similarly for the velocity and acceleration. By substituting the velocity and acceleration of tethers obtained from equation (50) into equation (40) and then into equation (36) together with equation (39), the equation of motion for the platform in accounting for the interactions among the platform, wave and tethers is written as

$$\begin{aligned}
&M\frac{d^2\xi}{dt^2} + K^*\xi \\
&= \rho_w \int_{-d}^{0} \left(\frac{\partial(\phi_i + \phi_{Is})}{\partial t}\bigg|_{x=-b} - \frac{\partial \phi_{IIIs}}{\partial t}\bigg|_{x=b} \right) dz + \rho_w \int_{-d}^{0} \left[\frac{\partial \phi_{Iw}}{\partial t}\bigg|_{x=-b} - \frac{\partial \phi_{IIIw}}{\partial t}\bigg|_{x=b} \right) dz \\
&\quad + \rho_w D\sigma \int_{-h}^{-d} R_d \left(-\frac{\partial \phi_{IIs}}{\partial x}\bigg|_{x=-b+\varepsilon} \right) dz + \rho_w D\sigma^2 (0{\cdot}25\pi D(C_m - 1) + iR_d^*)\lambda_1|_{x=-b+\varepsilon} \\
&\quad + \rho_w D\sigma \int_{-h}^{d} R_d \left(-\frac{\partial \phi_{IIw}}{\partial x}\bigg|_{x=-b+\varepsilon} \right) dz \\
&\quad + \rho_w D\sigma \int_{-h}^{-d} R_d \left(-\frac{\partial \phi_{IIs}}{\partial x}\bigg|_{x=b-\varepsilon} \right) dz + \rho_w D\sigma^2 (0{\cdot}25\pi D(C_m - 1) + iR_d^*)\lambda_2|_{x=b-\varepsilon} \\
&\quad + \rho_w D\sigma \int_{-h}^{-d} R_d \left(-\frac{\partial \phi_{IIw}}{\partial x}\bigg|_{x=-b-\varepsilon} \right) dz,
\end{aligned} \tag{51}$$

where $R_d = R_d^* - 0{\cdot}25\mathrm{i}D\pi C_m$, and

$$\lambda_1 = \frac{C_1}{a}(\mathrm{e}^{-ad} - \mathrm{e}^{-ah}) + \frac{-C_2}{a}(\mathrm{e}^{ad} - \mathrm{e}^{dh}) + \sum_{n=1}^{\infty} \frac{a_n}{K_{\mathrm{II}n}} \sin K_{\mathrm{II}n}(h-d), \tag{52}$$

$$\lambda_2 = \frac{C_1^*}{a}(\mathrm{e}^{-ad} - \mathrm{e}^{-ah}) + \frac{-C_2^*}{a}(\mathrm{e}^{ad} - \mathrm{e}^{dh}) + \sum_{n=1}^{\infty} \frac{a_n^*}{K_{\mathrm{II}n}} \sin K_{\mathrm{II}n}(h-d). \tag{53}$$

In the equation presented above, the external forces include the wave forces on the large body induced from the incoming incident waves and scattering waves and wave forces on the small body of the inertia and the drag forces. The subscript w denotes the radiated wave effect, from which two kinds of damping were induced: firstly, the radiated damping from the incident wave that may bring the energy away from the floating structure so that the structural vibration would not amplify continuously; secondly, the energy-dissipating damping from the fluid drags on the tethers that due to the vibration of the tether would actually damp the energy of the incident waves. Therefore, due to this hydraulic drag damping effect, the energy is not conserved for the incident waves. There exists a similar situation for the scattering waves. The equation of motion for the platform must be solved simultaneously with the scattering problems. After carrying out the necessary integration and separating the known terms from unknowns the final equation becomes

$$\begin{aligned}
&- \rho_W \left[\sum_{n=1}^{\infty} \frac{(-\mathrm{i}g)}{\cos K_n h} \langle Z_n^0 \rangle \right] A_{\mathrm{I}wn} - [\varsigma_1 + \varsigma_1^*] A_{\mathrm{II}wPI} \\
&+ \left[\sum_{n=2}^{\infty} ((G_n - \beta\Gamma_n) + (G_n^* - \beta\Gamma_n^*)\mathrm{e}^{-2bK_{\mathrm{II}n}}) \right] A_{\mathrm{II}wPn} \\
&+ \left[\sum_{n=2}^{\infty} ((G_n - \beta\Gamma_n)\mathrm{e}^{-2bK_{\mathrm{II}n}} + (G_n^* - \beta^*\Gamma_n^*)) \right] A_{\mathrm{II}wNn} \\
&+ \rho_W \left[\sum_{n=1}^{\infty} \frac{(-\mathrm{i}g)}{\cos K_n h} \langle Z_n^0 \rangle \right] A_{\mathrm{III}wn} \\
&+ [K - \sigma^2 M - (\beta Q + \beta^* Q^*)] S \\
&= \rho_w \left[\frac{\mathrm{i}A_i g}{\cos K_1 h} \mathrm{e}^{K_1 b} \langle Z_1^0 \rangle \right] \\
&+ \rho_W \left[\sum_{n=1}^{\infty} \frac{(-\mathrm{i}g)}{\cos K_n h} \langle Z_n^0 \rangle \right] A_{\mathrm{I}sn} - [\varsigma_1 + \varsigma_1^*] A_{\mathrm{II}sPI} \\
&+ \left[\sum_{n=2}^{\infty} ((G_n - \beta\Gamma_n) + (G_n^* - \beta^*\Gamma_n^*)\mathrm{e}^{-2bK_{\mathrm{II}n}}) \right] A_{\mathrm{II}sPn} \\
&+ \left[\sum_{n=2}^{\infty} ((G_n - \beta\Gamma_n)\mathrm{e}^{-2bK_{\mathrm{II}n}} + (G_n^* - \beta^*\Gamma_n^*)) \right] A_{\mathrm{II}sNn} \\
&+ \rho_W \left[\sum_{n=1}^{\infty} \frac{(-\mathrm{i}g)}{\cos K_n h} \langle Z_n^0 \rangle \right] A_{\mathrm{III}sn},
\end{aligned} \tag{54}$$

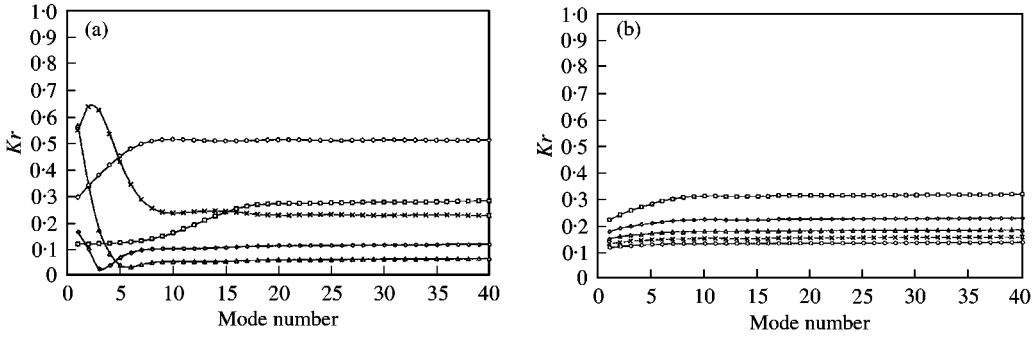

Figure 3. Convergence test on the reflection coefficient subject to: Nylon; $D = 5.08$ cm, $h = 20$ m, $b = 4$ m, $d = 2$ m, mass = 100 kg. (a) 2–10 s wave period: —□—, $T = 2$ s; —◇—, $T = 4$ s; —△—, $T = 6$ s; —×— $T = 8$ s; —○— $T = 10$ s. (b) 12–20 s wave period: —□—, $T = 12$ s; —◇—, $T = 14$ s, —△—, $T = 16$ s; —×— $T = 18$ s; —○— $T = 20$ s.

where the parameters β, β^*, Q, Q^*, Γ_n, Γ_n^*, ς_n, ς_n^*, G_n and G_n^* are all defined in Appendix C. With this equation combining the $4N$ boundary conditions together, solutions for these $4N + 1$ equations were carried out and then the motion of the platform, the motion of the pretension tethers and the unknown amplitudes for the velocity potential were obtained analytically.

4. NUMERICAL RESULTS AND DISCUSSIONS

To demonstrate the analytical solution, numerical examples were presented for both the platform motion and the reflection and transmission coefficients. The convergence test for the series of analytical solutions was also carried out. The period adopted for the incident waves in the numerical demonstration was varied from 2 to 20 s. The parameters being examined for the TLP system include the platform draft, platform width and mass, water depth, wave amplitude and the property and dimension of the tether. The following are numerical examples, where the dimensions of the TLP system under study are shown in the corresponding figures.

4.1. THE CONVERGENCE TEST OF THE ANALYTICAL SOLUTION

The convergence test was performed for the reflection coefficients when the wave period ranged from 2 s to 20 s. Shown in Figure 3(a) and (b) are the reflection coefficients corresponding to the mode numbers in the series of analytical solution; the number of modes needed for the convergence is about 15 and after that the reflection coefficient converges to a constant value.

4.2. INFLUENCE OF PLATFORM PARAMETERS ON THE DRAG SURGE MOTION

The parameters being examined here are the width, draft and the mass of the platform structure while the wave parameters and the tether material remain constant. The motion of the platform was studied and compared with the case without tether drag effect.

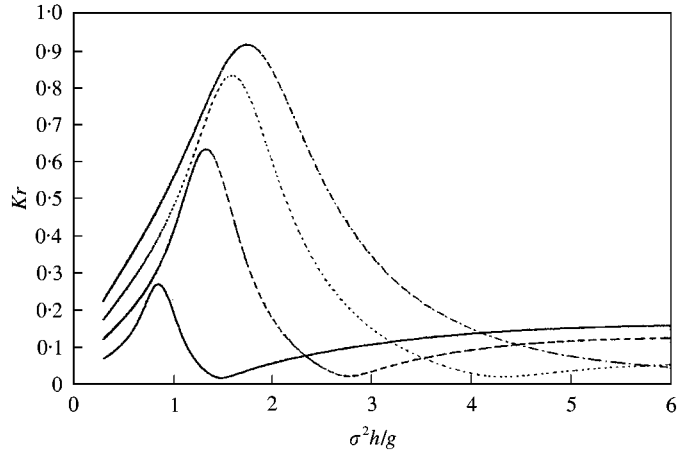

Figure 4. Reflection coefficient with respect to the platform width variation: Nylon; $D = 5.08$ cm, $d = 5.08$ cm, $d = 2$ m, $h = 20$ m, mass = 1000 kg; ——, $b = 2$ m; – – –, $b = 4$ m; ·····, $b = 6$ m; –·–·, $b = 8$ m.

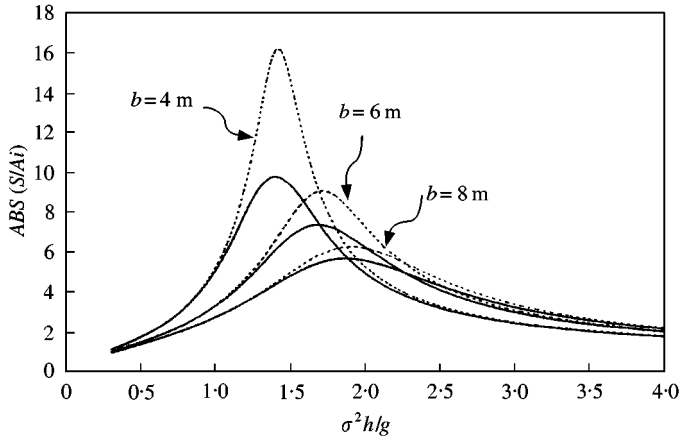

Figure 5. Comparison of dimensionless amplitude of platform with respect to width variation: Nylon; $D = 5.08$ cm, $d = 5.08$ cm, $d = 2$ m, $h = 20$ m, mass = 1000 kg; ——, with tether drag; ·····, no tether drag.

4.2.1. *Platform width on the drag surge motion*

Presented in Figure 4 is the reflection coefficient corresponding to the dimensionless wave frequency when the TLP system is subjected to the variation of the platform width. Corresponding to the increase of the platform width both the resonant frequency and the reflection coefficient increase. It is clear that the increase of the platform width will enhance the wave reflection effect and also the pretension stiffness for the system and therefore, the system resonant frequency is increased.

Figure 5 shows a comparison of the dimensionless amplitude for the platform motion corresponding to the variation of the platform width while the drag effect of tether was being examined. When the platform width increases the vibration amplitude is reduced no matter if the tether drag effect is considered or not. However, the tether drag will reduce the vibration amplitude, particularly when the platform width is small. Once the platform width is large the tether drag effect becomes insignificant. This is due to the fact that when the

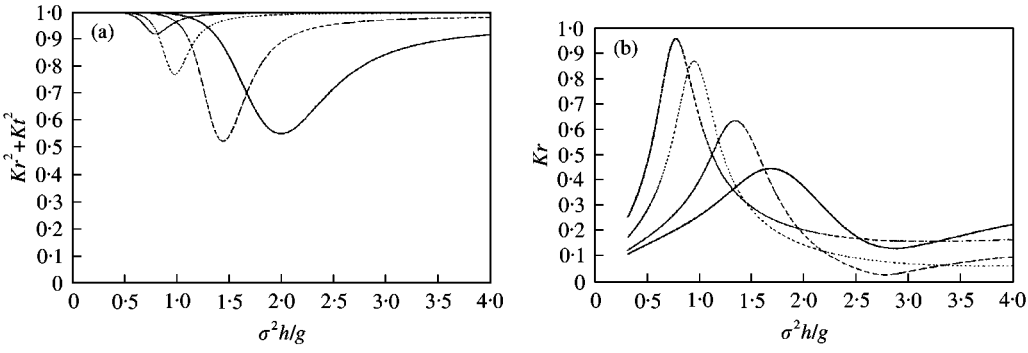

Figure 6. Nylon; $D = 5.08$ cm, $b = 4$ m, $h = 20$ m, mass $= 1000$ kg; (a) Square sum of reflection and transmission coefficient with respect to draft variation, (b) reflection coefficient with respect to the draft variation: ——, $d = 1$ m; – – –, $d = 2$ m; ·····, $d = 4$ m; –·–·, $d = 6$ m.

platform width is larger the wave transmitted is less which reduces the wave forces exerted on the tether and additionally, the larger platform width increases the pretension force on the tether that prevents the vibration of the tether. When the vibration is not significant the drag effect is mitigated too.

4.2.2. *Platform draft on the drag surge motion*

Figure 6(a) illustrated the square sum of reflection and transmission coefficient and Figure 6(b) presents the variation of the reflection coefficient corresponding to the dimensionless wave frequency when the TLP system is subjected to draft variation in a drag surge motion. Corresponding to the increase of the platform draft the reflection coefficient increases while the resonant frequency is reduced. Similar to the increase of the platform width, the increase of the draft will enhance the reflection effect, but for the influence on the resonant frequency, larger draft will put more added mass on the system so that the resonant frequency is reduced.

Figure 7 shows a comparison for the dimensionless amplitude of the platform motion while the drag effect of tether was being examined corresponding to the variation of the platform draft from 1 to 6 m. For the motion without considering the tether drag effect, the platform amplitude generally reduced corresponding to the increase of the draft but this is not the case when the tether drag effect was included. As is shown by the solid line in the figure the tether drag effect would reduce the vibration amplitude particularly when the draft is small. Once the draft is large, due to the same reason that the draft increment increases the pretension force on the tether, the drag effect of the tether becomes insignificant. However, unlike the case of the width variation, the dragged surge response is not monotonically related to the platform draft. There is an ultimate response corresponding to the variation of platform draft when other parameters remain the same.

4.2.3. *Platform mass on the drag surge motion*

For the mass variation effect Figure 8 shows the reflection coefficient and Figure 9 shows the dimensionless response amplitude corresponding to the dimensionless wave frequency. With respect to the increase of the mass, the response amplitude is increased while the reflection coefficient is reduced and the resonant frequency moves to the low value range. It is well-known that the increase of the platform mass reduces the system frequency. The increase of the response amplitude is due to the increase of the initial draft that reduces the equivalent stiffness of the system and the reflection coefficient is reduced when more

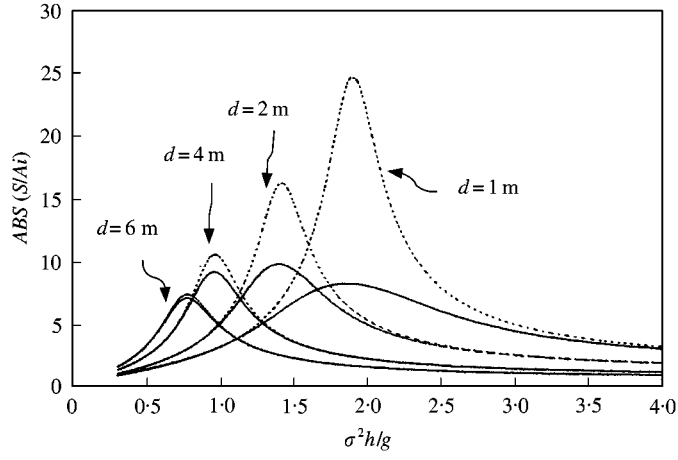

Figure 7. Comparison of dimensionless amplitude of platform with respect to draft variation Nylon; $D = 5.05$ cm, $b = 4$ m, $h = 20$ m, mass = 1000 kg; ——, with tether effect; ·····, no tether effect.

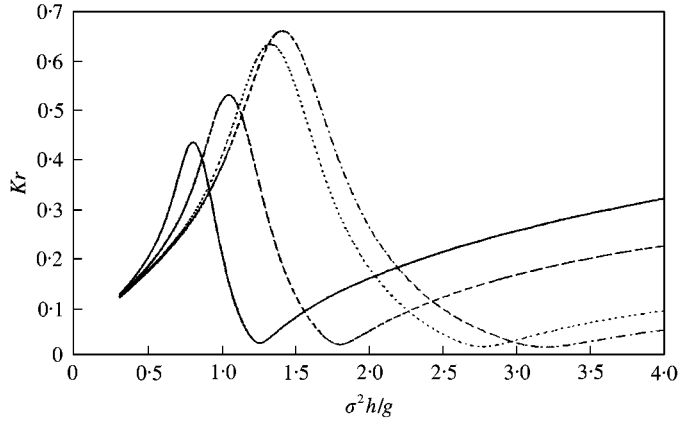

Figure 8. Reflection coefficient with respect to mass variation: Nylon; $D = 5.08$ cm, $b = 4$ m, $d = 2$ m, $h = 20$ m; –·—·, $M = 500$ kg; ·····, $M = 1000$ kg; – – –, $M = 3000$ kg; ——, $M = 5000$ kg.

platform excitation is allowed. The tether drag effect is more obvious when the structure mass is larger.

4.3. INFLUENCE OF WATER WAVE ON THE DRAG SURGE MOTION

The parameter of water depth and the amplitude of the incident wave were examined here. The comparison of the response amplitude between the cases with and without the tether drag effect was presented and the coefficient of the reflection and the transmission was also further studied.

4.3.1. *Water depth on the drag surge motion*

The response amplitude of the platform system under various water depths was presented in Figure 10, whether the water depth varied from 10 to 30 m. When the water is deep the difference between the platform with and without considering the tether drag effect is large

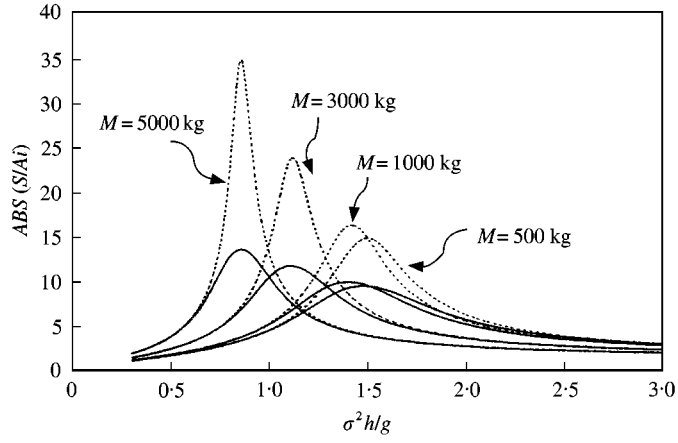

Figure 9. Comparison of dimensionless amplitude of platform with respect to mass variation: Nylon; $D = 5.08$ cm, $b = 4$ m, $d = 2$ m, $h = 20$ m; ——, with tether drag; ·····, no tether drag.

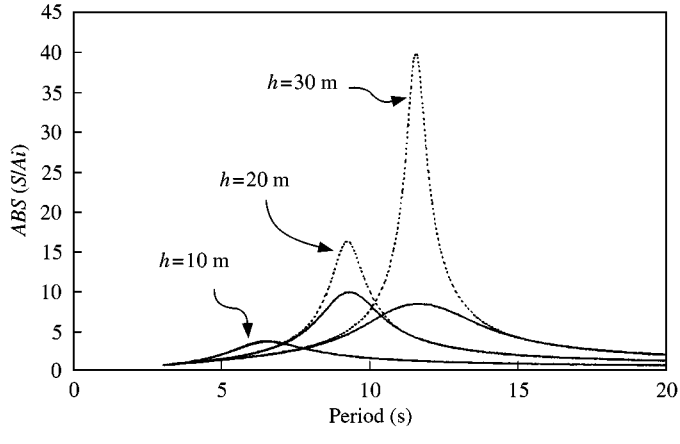

Figure 10. Comparison of dimensionless amplitude of platform with respect to water depth. Nylon; $D = 5.08$ cm, $b = 4$ m, $d = 2$ m, mass = 1000 kg; ——, with tether drag; ·····, no tether drag.

while in the shallow water case the difference becomes small. It is because when the water is deep the tether needed to anchor the platform structure is longer and subjected to more severe wave motions that consumes more energy input into the TLP system and then reduces the response of the platform. However, this phenomenon similar to that found in the case of the platform draft variation is not linearly related to the depth variation. It is due to the more complicated cause that the change of water depth will not only influence the stiffness of the platform system but also affect the wavelength and subsequently, the related flow field.

4.3.2. *Wave amplitude on the drag surge motion*

Figure 11(a) and 11(b) present the square sum of the reflection and transmission coefficient and the reflection coefficient itself when the amplitude of the incident wave is a variable. In this case the coefficient of platform without considering the tether drag is also shown in the figure, where as shown in Figure 11(a) the square sum of the reflection and the

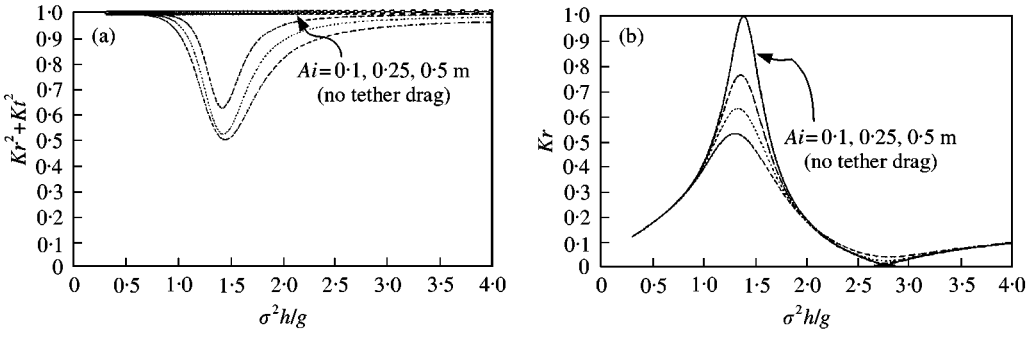

Figure 11. Nylon; $D = 5.08$ cm, $b = 4$ m, $d = 2$ m, mass = 1000 kg; (a) Square sum of reflection and transmission coefficient with respect to wave amplitude; (b) reflection coefficient with respect to wave amplitude: – – –, $Ai = 0{\cdot}1$ m; ·····, $Ai = 0{\cdot}25$ m; – · –, $Ai = 0{\cdot}5$ m.

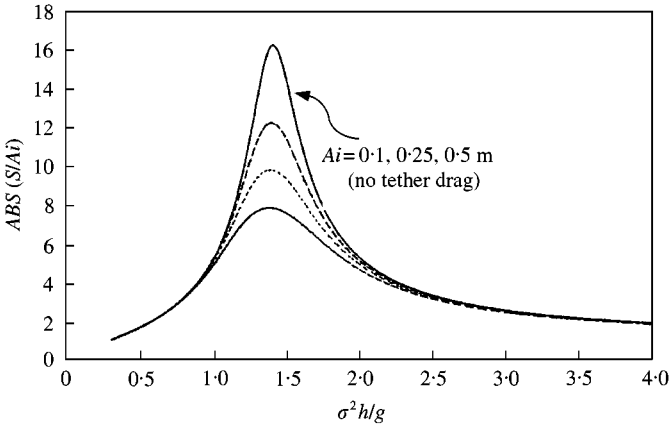

Figure 12. Comparison of dimensionless amplitude of platform with respect to wave amplitude. Nylon; $D = 5.08$ cm, $b = 4$ m, $d = 2$ m, mass = 1000 kg; – – –, $Ai = 0{\cdot}1$ m; ·····, $Ai = 0{\cdot}25$ m; – · –, $Ai = 0{\cdot}5$ m.

transmission coefficient is a unit quantity no matter what the amplitude of the incident wave is. When the tether drag was accounted for corresponding to the increase of the wave amplitude the reflection coefficient increases. Figure 12 shows the response amplitude of the platform, where the response decreases corresponding to the increase of the wave amplitude. This is because the particle velocity corresponding to the increased wave amplitude amplifies the drag effect on the tethers that reduces the platform motion.

4.4. INFLUENCE OF TETHER PARAMETERS ON THE DRAG SURGE MOTION

Three types of material were used for analysis, namely, Polyethylene, Nylon and GFRP, of which the elastic modulis are 0·7, 2·0 and 7·0 GPa respectively. The effect of the diameter of the tether was also studied here.

4.4.1. *Tether material on the drag surge motion*

When the material of the tether is varied the behavior of the drag motion of the platform is also changed. Figure 13 shows the variation of the reflection coefficient for the system

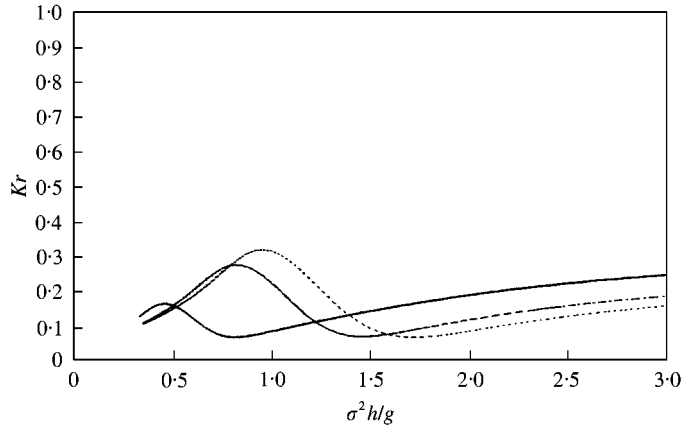

Figure 13. Reflection coefficient with respect to the variation of material amplitude. Nylon; $D = 5.08$ cm, $b = 4$ m, $d = 2$ m, $h = 30$ m, mass = 1000 kg; ——, polyethylene; – · – · –, nylon; · · · · · ·, GFRP.

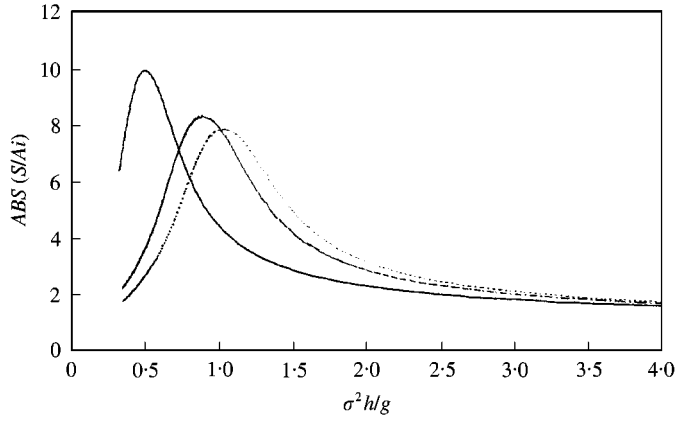

Figure 14. Comparison of dimensionless amplitude of platform with respect to variation of material property: Nylon; $D = 5.08$ cm, $b = 4$ m, $d = 2$ m, $h = 30$ m, mass = 1000 kg; ——, polyethylene; – · – · –, nylon; · · · · · ·, GFRP.

with respect to the wave frequency, where corresponding to the increase of the elastic modulus of the material the reflection coefficient decreases while the resonant frequency increases. Figure 14 shows the dimensionless response amplitude of the platform, where the drag amplitude decreases corresponding to the increase of the elastic modulus. It is clear that the increase of the elastic modulus increases the system stiffness and the resonant frequency.

4.4.2. *Tether dimension on the drag surge motion*

Presented in Figure 15 is the comparison of the dimensionless response amplitude for the platform system with and without considering the tether drag effect when the diameter of the tether is varied. It shows that corresponding to the increase of the tether diameter the response is reduced and the tether drag has significant influence on the responses. The difference between the platform system with and without tether drag is significant no matter how large the tether diameter is as long as the material is the same.

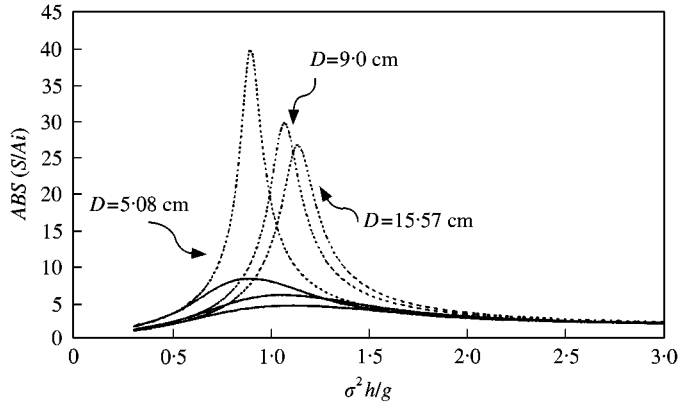

Figure 15. Comparison of dimensionless amplitude of platform with respect to the variation of tension-leg tether diameter. Nylon; $b = 4$ cm, $d = 2$ m, $h = 30$ m, mass $= 1000$ kg; ——, with tether drag; ·····, no tether drag.

5. CONCLUSIONS

A set of equations to describe the drag surge motion for the platform and the tether of tension leg were derived. The corresponding close form analytical solution was obtained as an infinite series for the dynamic behavior of both the platform subjected to the wave-induced surge motion and the tethers subjected to the flow-induced drag motion. The solution of infinite series was first examined in the convergence test for the reflection coefficient and then demonstrated in the numerical examples in accounting for the variation of the parameters of the platform, wave and the tethers.

In the comparisons for the response between drag surge and surge motion it showed that the tether drag would significantly reduce the responses in general. However, when the parameters of the platform or wave or tethers varied, the drag effect was influenced. In the consideration of platform parameters, the tether drag is very significant for platform with small draft or dimension. The tether drag effect is also more obvious when the platform mass is larger. However, when the draft or dimension of the platform is large the drag effect of the tethers becomes insignificant. In the variation of water depth, the tether drag is more significant for platform system located at shallow water. Corresponding to the increase of the wave amplitude, the drag surge response of the platform is decreased. For the tethers of varied material or dimensions, the drag surge motion of the platform is decreased corresponding to the increase of the dimension or elastic modulus.

Therefore, we may conclude that the traditional analysis on the tension-leg platform system without considering interactions of the drag effect of the tether legs tends to overestimate the vibration amplitude for the platform when the draft or dimension of the platform is small or when the structural mass is large.

ACKNOWLEDGMENT

This study was partially supported by the National Science Council, Taiwan under grant No. 88-2611-E-110-008. It is gratefully acknowledged here.

REFERENCES

1. C. J. GARRISON 1974 *OTC* 2067 Dynamic response of floating bodies. 365–378.
2. T. SARPKAYA and M. ISAACSON 1981 *Mechanics of wave forces on offshore structures*, New York: Van Nostrand Reinhold.
3. C. C. MEI 1978 *Annual Review of Fluid Mechanics* **10**, 393. Numerical methods in water wave diffraction and radiation.
4. T. YAMAMOTO, A. YOSHIDA and T. IJIMA 1982 in *Dynamics Analysis of Offshore Structures* (C. L. KIRK, editor). Southampton: CML. Dynamics of elastically moored floating objects.
5. C.-P. LEE and J.-F. LEE 1993 *Ocean Engineering* **20**, 171–186. Wave induced surge motion of a tension leg structure.
6. A. K. JAIN 1997 *Ocean Engineering* **24**, 577–592. Nonlinear coupled response of offshore tension leg platforms to regular wave forces.
7. P. C. CHATTERJEE, P. K. DAS and D. FAULKNER 1997 *Ocean Engineering* **24**, 313–333. A hydro-structural analysis program for TLPs.
8. C.-P. LEE 1994 *Ocean Engineering* **21**, 311–328. Dragged surge motion of a tension leg structure.
9. H. H. LEE, P.-W. WANG and C.-P. LEE 1999 *Ocean Engineering* **26**, 575–594. Dragged surge motion of tension leg platforms and strained elastic tethers.
10. J. L. BLACK, C. C. MEI and M. C. G. BRAY 1971 *Journal of Fluid Mechanics* **46**, 151–164. Radiation and scattering of water waves by rigid bodies..
11. H. H. LEE and P.-W. WANG 2000 *Ocean Engineering* **27**, 393–415. Analytical solution on the surge motion of tension leg twin-platform structural system (in press).
12. J. N. NEWMAN 1977 *Marine Hydrodynamics*. Cambridge, Massachussetts: MIT Press.
13. J. R. MORISON, M. P. O'BRIEN, J. W. JOHNSON and S. A. SCHAAF 1950 *Petroleum Transactions AIME*, **189**, 149–154. The force exerted by surface waves on piles.
14. R. G. DEAN and R. A. DALRYMPLE 1991. *Water Waves Mechanics for Engineers and Scientists*. Singapore: World Scientific.
15. C. K. SOLLIITT and R. H. CROSS 1972 *Proceedings of* 13*th ICCE*, *ASCE*. Wave transmission through permeable breakwaters.

APPENDIX A

$$\langle Z_n Z_\alpha \rangle = \int_{-h}^{0} \cos[K_n(z+h)] \cos[K_\alpha(z+h)]\,\mathrm{d}z$$

$$= \begin{cases} 0, & n \neq \alpha, \\ \dfrac{h}{2}\left[1 + \dfrac{\sinh(2K_\alpha h)}{2K_\alpha h}\right], & n = \alpha, \end{cases} \tag{A1}$$

$$\langle Z_{\mathrm{II}n} Z_\alpha \rangle^d = \int_{-h}^{-d} \cos[K_{\mathrm{II}n}(z+h)] \cos[K_\alpha(z+h)]\,\mathrm{d}z$$

$$= \begin{cases} \dfrac{h-d}{2}\left\{1 + \dfrac{\sin[2K_\alpha(h-d)]}{2K_\alpha h}\right\}, & K_{\mathrm{II}n} = K_\alpha, \\ \dfrac{1}{2}\left\{\dfrac{\sin[(K_{\mathrm{II}n} + K_\alpha)(h-d)]}{K_{\mathrm{II}n} + K_\alpha} + \dfrac{\sin[(K_{\mathrm{II}n} - K_\alpha)(h-d)]}{K_{\mathrm{II}n} - K_\alpha}\right\}, & K_{\mathrm{II}n} \neq K_\alpha, \end{cases} \tag{A2}$$

$$\langle Z_{\mathrm{II}n} Z_{\mathrm{II}\alpha} \rangle^d = \int_{-h}^{d} \cos[K_{\mathrm{II}n}(z+h)] \cos[K_{\mathrm{II}\alpha}(z+h)]\,\mathrm{d}z$$

$$= \begin{cases} 0, & n \neq \alpha, \\ h-d, & n = \alpha = 1, \\ \dfrac{h-d}{2}, & n = \alpha \neq 1, \end{cases} \tag{A3}$$

$$\langle Z_n^0 \rangle = \int_{-d}^{0} \cos[K_n(z+h)]\,\mathrm{d}z,$$

$$= \frac{1}{K_n}[\sin K_n h - \sin K_n(h-d)]. \tag{A4}$$

APPENDIX B

$$a = \pm\sqrt{-\frac{1}{T^*}\{\sigma^2[\rho^* + 0{\cdot}25\pi\rho_w D^2(C_m-1)] + \mathrm{i}\sigma(C + R_{d1}^{**}\rho_w D\sigma)\}}, \tag{B1}$$

$$a^* = \pm\sqrt{-\frac{1}{T^*}\{\sigma^2[\rho^* + 0{\cdot}25\pi\rho_w D^2(C_m-1)] + \mathrm{i}\sigma(C + R_{d2}^{**}\rho_w D\sigma)\}}, \tag{B2}$$

$$C_1 = \frac{1}{\mathrm{e}^{a(h-d)} - \mathrm{e}^{-a(h-d)}}\left\{\mathrm{e}^{ah}\left[S - \sum_{n=1}^{\infty} a_n \cos K_{\mathrm{II}n}(h-d)\right] + \mathrm{e}^{ad}\sum_{n=1}^{\infty} a_n\right\}, \tag{B3}$$

$$C_1^* = \frac{1}{\mathrm{e}^{a^*(h-d)} - \mathrm{e}^{-a^*(h-d)}}\left\{\mathrm{e}^{a^*h}\left[S - \sum_{n=1}^{\infty} a_n^* \cos K_{\mathrm{II}n}(h-d)\right] + \mathrm{e}^{a^*d}\sum_{n=1}^{\infty} a_n^*\right\}, \tag{B4}$$

$$C_2 = \frac{1}{\mathrm{e}^{a(h-d)} - \mathrm{e}^{-a(h-d)}}\left\{\mathrm{e}^{-ah}\left[\sum_{n=1}^{\infty} a_n \cos K_{\mathrm{II}n}(h-d) - S\right] - \mathrm{e}^{-ad}\sum_{n=1}^{\infty} a_n\right\}, \tag{B5}$$

$$C_2^* = \frac{1}{\mathrm{e}^{a^*(h-d)} - \mathrm{e}^{-a^*(h-d)}}\left\{\mathrm{e}^{-a^*h}\left[\sum_{n=1}^{\infty} a_n^* \cos K_{\mathrm{II}n}(h-d) - S\right] - \mathrm{e}^{-a^*d}\sum_{n=1}^{\infty} a_n^*\right\}, \tag{B6}$$

$$a_1 = \frac{A_{\mathrm{II}s/wPI}(0{\cdot}25\pi\rho_w C_m D^2 g + \mathrm{i}\rho_w D R_{d1}^{**} g)}{b\{\sigma^2[\rho^* + 0{\cdot}25\pi\rho_w D^2(C_m-1)] + \mathrm{i}\sigma(C + R_{d1}^{**}\rho_w D\sigma)\}}, \tag{B7}$$

$$a_1^* = \frac{A_{\mathrm{II}s/wPI}(0{\cdot}25\pi\rho_w C_m D^2 g + \mathrm{i}\rho_w D R_{d2}^{**} g)}{b\{\sigma^2[\rho^* + 0{\cdot}25\pi\rho_w D^2(C_m-1)] + \mathrm{i}\sigma(C + R_{d2}^{**}\rho_w D\sigma)\}}, \tag{B8}$$

$$a_n = \frac{1}{-T^*(K_{\mathrm{II}n})^2 + \sigma^2[\rho^* + 0{\cdot}25\pi\rho_w D^2(C_m-1)] + \mathrm{i}\sigma(C + R_{d1}^{**}\rho_w D\sigma)}$$

$$\times (0{\cdot}25\pi\rho_w D^2 C_m g + \mathrm{i}\rho_w D R_{d1}^{**} g)(-1)^{n-1}(-K_{\mathrm{II}n}A_{\mathrm{II}s/wPn}\mathrm{e}^{-\varepsilon K_{\mathrm{II}n}} + K_{\mathrm{II}n}A_{\mathrm{II}s/wNn}\mathrm{e}^{-(2b-\varepsilon)K_{\mathrm{II}n}}),$$

$$n \geqslant 2, \tag{B9}$$

$$a_n^* = \frac{1}{-T^*(K_{\mathrm{II}n})^2 + \sigma^2[\rho^* + 0{\cdot}25\pi\rho_w D^2(C_m - 1)] + \mathrm{i}\sigma(C + R_{d2}^{**}\rho_w D\sigma)}$$
$$\times (0{\cdot}25\pi\rho_w D^2 C_m g + \mathrm{i}\rho_w D R_{d2}^{**} g)(-1)^{n-1}(-K_{\mathrm{II}n}A_{\mathrm{IIs/w}Pn}\mathrm{e}^{-(2b-\varepsilon)K_{\mathrm{II}n}} + K_{\mathrm{II}n}A_{\mathrm{IIs/w}Nn}\mathrm{e}^{-\varepsilon K_{\mathrm{II}n}}),$$
$$n \geqslant 2. \tag{B10}$$

APPENDIX C

$$\beta = \rho_w D\sigma^2[0{\cdot}25\pi D(C_m - 1) + \mathrm{i}R_{d1}^*], \tag{C1}$$

$$\beta^* = \rho_w D\sigma^2[0{\cdot}25\pi D(C_m - 1) + \mathrm{i}R_{d2}^*], \tag{C2}$$

$$Q = \frac{\mathrm{e}^{a(d-h)} + \mathrm{e}^{-a(d-h)} - 2}{a[\mathrm{e}^{a(h-d)} - \mathrm{e}^{-a(h-d)}]}, \tag{C3}$$

$$Q^* = \frac{\mathrm{e}^{a^*(d-h)} + \mathrm{e}^{-a^*(d-h)} - 2}{a^*[\mathrm{e}^{a^*(h-d)} - \mathrm{e}^{-a^*(h-d)}]}, \tag{C4}$$

$$\Gamma_n = \frac{\mathrm{e}^{-ad} - \mathrm{e}^{-ah}}{a}\frac{1}{v}[-\mathrm{e}^{ah}\varsigma_n\cos[K_{\mathrm{II}n}(h-d)] + \mathrm{e}^{ad}\varsigma_n]$$
$$+ \frac{-(\mathrm{e}^{ad} - \mathrm{e}^{ah})}{a}\frac{1}{v}[\mathrm{e}^{-ah}\varsigma_n\cos[K_{\mathrm{II}n}(h-d)] - \mathrm{e}^{ad}\varsigma_n]$$
$$+ \frac{\sin[K_{\mathrm{II}n}(h-d)]}{K_{\mathrm{II}n}}\varsigma_n, \quad n \geqslant 2, \tag{C5}$$

where $v = \mathrm{e}^{a(h-d)} - \mathrm{e}^{-a(h-d)}$,

$$\Gamma_n^* = \frac{\mathrm{e}^{-a^*d} - \mathrm{e}^{-a^*h}}{a^*}\frac{1}{v^*}[-\mathrm{e}^{a^*h}\varsigma_n^*\cos[K_{\mathrm{II}n}(h-d)] + \mathrm{e}^{a^*d}\varsigma_n^*]$$
$$+ \frac{-(\mathrm{e}^{a^*d} - \mathrm{e}^{a^*h})}{a^*}\frac{1}{v^*}[\mathrm{e}^{-a^*h}\varsigma_n^*\cos[K_{\mathrm{II}n}(h-d)] - \mathrm{e}^{-a^*d}\varsigma_n^*]$$
$$+ \frac{\sin[K_{\mathrm{II}n}(h-d)]}{K_{\mathrm{II}n}}\varsigma_n^*, \quad n \geqslant 2, \tag{C6}$$

where $v^* = \mathrm{e}^{a^*(h-d)} - \mathrm{e}^{-a^*(h-d)}$,

$$\varsigma_n = \frac{(-1)^{n-1}[0{\cdot}25\pi\rho_W D^2 C_m g + \mathrm{i}\rho_w D R_{d1}^* g](K_{\mathrm{II}n})}{-T^*(K_{\mathrm{II}n})^2 + \sigma^2[\rho^* + 0{\cdot}25\pi\rho_w D^2(C_m - 1)] + \mathrm{i}\sigma(C + R_{d1}^*\rho_w D\sigma)}, \quad n \geqslant 2, \tag{C7}$$

$$\varsigma_n^* = \frac{(-1)^{n-1}[0{\cdot}25\pi\rho_W D^2 C_m g + \mathrm{i}\rho_w D R_{d2}^* g](K_{\mathrm{II}n})}{-T^*(K_{\mathrm{II}n})^2 + \sigma^2[\rho^* + 0{\cdot}25\pi\rho_w D^2(C_m - 1)] + \mathrm{i}\sigma(C + R_{d2}^*\rho_w D\sigma)}, \quad n \geqslant 2, \tag{C8}$$

$$\varsigma_1 = \frac{[0{\cdot}25\pi\rho_W D^2 C_m g + \mathrm{i}\rho_w D R_{d1}^* g]\cos[K_{\mathrm{III}}(h-d)]}{avb\sigma^2[\rho^* + 0{\cdot}25\pi\rho_w D^2(C_m - 1)] + \mathrm{i}\sigma(C + R_{d1}^*\rho_w D\sigma)}[2 - \mathrm{e}^{a(h-d)} - \mathrm{e}^{a(d-h)}]$$
$$+ \frac{[0{\cdot}25\pi\rho_W D^2 C_m g + \mathrm{i}\rho_w D R_{d1}^* g]}{avb\sigma^2[\rho^* + 0{\cdot}25\pi\rho_w D^2(C_m - 1)] + \mathrm{i}\sigma(C + R_{d1}^*\rho_w D\sigma)}[2 - \mathrm{e}^{a(h-d)} - \mathrm{e}^{a(d-h)}], \tag{C9}$$

$$\varsigma_1^* = \frac{[0{\cdot}25\pi\rho_W D^2 C_m g + \mathrm{i}\rho_w D R_{d2}^* g]\cos[K_{\mathrm{III}}(h-d)]}{a^* v^* b\sigma^2[\rho^* + 0{\cdot}25\pi\rho_w D^2(C_m - 1)] + \mathrm{i}\sigma(C + R_{d2}^*\rho_w D\sigma)}[2 - \mathrm{e}^{a^*(h-d)} - \mathrm{e}^{a^*(d-h)}]$$

$$+ \frac{[0{\cdot}25\pi\rho_W D^2 C_m g + \mathrm{i}\rho_w D R_{d2}^* g]}{a^* v^* b\sigma^2[\rho^* + 0{\cdot}25\pi\rho_w D^2(C_m - 1)] + \mathrm{i}\sigma(C + R_{d2}^*\rho_w D\sigma)}[2 - \mathrm{e}^{a^*(d-h)} - \mathrm{e}^{a^*(h-d)}], \tag{C10}$$

$$G_n = \rho_w D\sigma R_{d1}(-1)^{n-1}\sin[K_{\mathrm{II}n}(h-d)]\mathrm{i}g/\sigma, \quad n \geqslant 2, \tag{C11}$$

$$G_n^* = \rho_w D\sigma R_{d2}(-1)^{n-1}\sin[K_{\mathrm{II}n}(h-d)]\mathrm{i}g/\sigma, \quad n \geqslant 2. \tag{C12}$$